Biosensors and Bioelectronics 144 (2019) 111668

Contents lists available at ScienceDirect

Biosensors and Bioelectronics

journal homepage: www.elsevier.com/locate/bios

Amplification of aptamer sensor signals by four orders of magnitude via interdigitated organic electrochemical transistors

Yuanying Liang, Changtong Wu, Gabriela Figueroa-Miranda, Andreas Offenhäusser, Dirk Mayer*

Institute of Complex Systems, Bioelectronics (ICS-8) and JARA-Fundamentals of Future Information Technology, Forschungszentrum Jülich, 52425, Jülich, Germany

ARTICLE INFO

Keywords:
Electrochemical signal amplification
Interdigitated organic electrochemical transistors
Aptasensor
Potentiometric transducer
Adenosine triphosphate

ABSTRACT

Electrochemical aptamer receptor/transducer systems are key elements of emerging E-AB sensors (aptasensor) used for the detection of various kinds of targets. However, the performance of these amperometric sensors is often limited by the low density of receptors attached to the sensor surface and high background signals. In the present work, interdigitated organic electrochemical transistors (iOECT) were used as a transducer to enhance the sensitivity and dynamic detection range of aptasensors. Therefore, the electrode of an amperometric sensor was utilized as gate electrode to operate the iOECT. This device was used to detect the low weight target molecule adenosine triphosphate (ATP), a common biomarker, which plays an important role for cardiovascular, neurodegenerative, and immune deficiency diseases. The novel aptasensor can selectively detect ATP with ultrahigh sensitivity down to the concentration of 10 pM, which is four orders of magnitude lower than the detection limit of the same aptasensor using an amperometric transducer principle (limit-of-detection of 106 nM) and most other previously reported electrochemical sensors. Furthermore, sensor regeneration was demonstrated, which facilitates reusability of OECT aptasensors. The small device size in combination with high transconductances paves the way for the development of highly sensitive integrated micro-biosensors for point-of-care applications.

1. Introduction

The detection of disease-related biomarkers is a primary goal of bioanalytical chemistry, which seeks to determine a certain analyte at very low concentrations to enable an early diagnosis. For the development of highly sensitive and selective biosensors, two functional components are crucial. One is the target recognition element (receptor) and the other one is the signal conversion unit (transducer). Aptamer receptors-based biosensors (aptasensors) have rapidly gained in importance because of their high affinity, selectivity, low cost, and easy-fabrication (Tan et al., 2013) (Privett et al., 2010). Various types of transduction principles have been exploited for aptasensors determining mass changes (e.g. quartz crystal microbalance) (Gründler, 2007), optical (e.g. fluorimetric) (E Wang et al., 2011), and electrochemical signals (Feng et al., 2015b; Lai et al., 2007; Xiao et al., 2005a). Especially amperometric aptasensors are of interest since they are easy to assemble, compatible to point of care applications, reusable (Feng et al., 2016), and sensitive in a wide range of concentrations (Lubin and Plaxco, 2010). However, the low density of oligonucleotide receptors on the electrode surface significantly limits the detectable electrochemical signal since each receptor contributes with only a specific number of exchanged charge carriers per redox probe (n) to the current signal and the sensors usually do not support an intrinsic signal amplification (White et al., 2008). A few strategies have been proposed to enhance the sensor signals by exploiting nanomaterials, enzymes, or electrocatalytic redox tags (Feng et al. 2011, 2015b; Li et al., 2013b). For example, nanomaterials can amplify the signal by increasing the load with receptor molecules (Palchetti and Mascini, 2012). Alternatively, electrochemical current rectification enhances the amperometric signal remarkably by introducing solution-phase redox molecules that reactivate the aptamer bound redox probes (Feng et al. 2015a, 2015b). However, these approaches require complicated receptor modifications or detection processes. Consequently, developing simple signal amplification strategies remains a challenge to improve sensor performance and to meet the requirements of early disease diagnosis.

A promising alternative electrochemical transducer principle utilizes organic electrochemical transistors (OECTs) as an intrinsically amplifying unit to bust the sensitivity of the biosensor. OECTs possess additional benefits of device properties such as biocompatibility, simple processability, and straightforward operation in aqueous solution as an ion-to-electron converter (Bernards and Malliaras, 2007; Zeglio and

* Corresponding author.
E-mail address: dirk.mayer@fz-juelich.de (D. Mayer).

https://doi.org/10.1016/j.bios.2019.111668
Received 12 June 2019; Received in revised form 13 August 2019; Accepted 29 August 2019
Available online 30 August 2019
0956-5663/

Inganäs, 2018). These exceptional properties, together with simple signal readout, the inherent amplification function, and small device dimensions makes OECTs attractive in particular for lab-on-a-chip applications in chemical and biological sensing (Fu et al., 2017; Khodagholy et al., 2013a). Compared to conventional electrochemical approaches, the OECT-based biosensors have proven to outperform other state-of-the-art devices (Khodagholy et al., 2013a) and exhibit higher sensitivity for a wide range of targets including proteins (Fu et al., 2017; Kim et al., 2010) or even cells (Lin et al., 2010b) due to their high current modulation in response to changes of the gate potential. For example, Fu et al. fabricated an OECT-based biosensor for human epidermal growth factor receptor 2 by nanoprobe modified antibody receptors, which showed several orders of magnitude lower detection limit than previously reported electrochemical transducers (Fu et al., 2017). Braendlein et al. developed a Wheatstone bridge OECT circuit for ex vivo detection of lactate concentration (Braendlein et al., 2017b). Lin et al. used OECTs integrated into a flexible microfluidic system to detect complementary DNA targets (Lin et al., 2011). Saraf et al. introduced aptamer to selectively bind to epinephrine molecule whose oxidation caused the decrease of the channel current of OECT (Saraf et al., 2018). Chen et al. chose aptamer-modified gold nanoparticles to form a specific probe on the gate electrode of an OECT for the detection of glycan expression on living cells (Chen et al., 2018). However, these OECT-based sensors are complicated, expensive, and mainly used to detect heavy molecules, like proteins, while rapid, convenient, inexpensive, and OECT-based aptasensors detecting light molecules, to our knowledge, are still lacking mainly because light molecules have only little impact on the potential of gate electrodes at low concentrations.

In the present work, an interdigitated OECT (iOECT) was used to amplify the electrochemical signals of an aptasensor for ATP without utilizing any catalytic active material. ATP is the energy currency for all kinds of cells and therefore involved in multifarious biochemical processes. A deviation of the regular ATP level is often a side effect of an emerging disease. Therefore, ATP levels can provide adjuvant information for health examinations in addition to regular biomarkers and examination methods. Furthermore, monitoring ATP as co-substrate is crucial for process control in biosynthesis. Given the importance of ATP for healthcare, biology, and biotechnology, it was chosen as the model target molecule in this study and for comparing the performance of conventional amperometric transducer with iOECT aptasensors. The general binding process of the analyte to the aptamer receptor is practically the same for both sensor types. Once applying ATP to the respective sensor, the specific target-binding alters the conformation of aptamer, resulting in the changes of the aptamer conformation at the electrode surface, Fig. 1a. In the case of the amperometric transducer, this rearrangement leads to an alteration of the distance between a terminal redox group (ferrocene) attached at the distal end of the aptamer (the yellow dot at the aptamer, Fig. 1) and the electrode surface, which alters the charge transfer and generates a detectable electrochemical signal (Xiao et al., 2007).

The iOECT-transducer system comprises an ionic and an electronic circuit, Fig. 1b. The target-binding event occurs in the ionic part at the gate electrode based on the same recognition process described above for the amperometric transducer. This binding event alters the gate potential and thus causes changes of corresponding source-drain current in the electronic circuit. We found that a slight change of gate potential induced by ATP-binding can result in a distinct variation of transfer characteristics, which facilitates detection limits as small as 10 pM. This sensitivity is superior to most of the previously reported biosensors for ATP, which is a very light molecule and therefore difficult to detect in ultralow concentrations. Furthermore, the selectivity and regeneration performance of the aptasensor were evaluated and demonstrated.

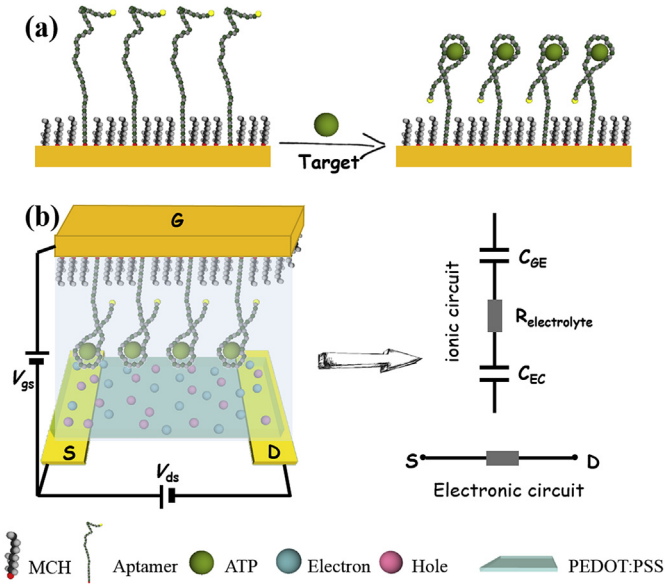

Fig. 1. Schematic illustration of the electrochemical response of two aptamer-based biosensors. In (a), an amperometric redox beacon aptamer sensor is illustrated where a gold electrode is modified with aptamer probes and blocking molecules MCH. A ferrocene redox group (Fc, yellow circle) attached to the distal end of the aptamer is reporting via charge transfer on a molecular recognition event involving a conformational change of the molecular beacon. (b) shows an iOECT with an aptamer-functionalized gate immersed in the electrolyte and the wiring for operating the sensor device (left). The conformational change of the aptamer on target binding is the same as in (a) Right: Two circuits for OECTs operation, ionic circuit and electronic circuit. C_{GE} and C_{EC} represent the capacitances of two electrical double layers at the gate/electrolyte interface and electrolyte/channel interface, respectively. (For interpretation of the references to colour in this figure legend, the reader is referred to the Web version of this article.)

2. Material and methods

2.1. Reagents

An ATP aptamer with the sequence of 5′-Ferrocene–$(CH_2)_6$–ACC TGG GGG AGT ATT GCG GAG GAA GGT–$(CH_2)_6$–SH-3′ was purchased from FRIZ Biochem (Neuried, Germany). The DNA probes were received as lyophilized powders and stored at −20 °C. The stock solution of DNA probes was prepared with 10 mM tris-EDTA buffer (pH 8.0). The concentration of aptamer in the stock solution was determined by using UV–vis spectroscopy to obtain the average absorbance value at 260 nm. Tris-(2-carboxyethyl) phosphine hydrochloride (TCEP), 6-mercapto-1-hexanol (MCH), adenosine triphosphate (ATP) and its analogs, dimethyl sulfoxide (DMSO), and 3-glycidoxypropyltrimethoxysilane (GOPS) were purchased from Sigma (Sigma-Aldrich Chemie GmbH, Germany) and used without further purification. Poly(3,4-ethylenedioxythiophene) doped with poly(styrenesulfonate) (PEDOT:PSS) solution (Clevios PH1000, Heraeus Clevios GmbH, Germany) was filtered by 0.8 μm filter before use. A glass ring with an outer diameter of 20 mm and a height of 10 mm was glued on the chip by polydimethylsiloxane (PDMS, Dow Corning Corporation, Germany) with a mixing ratio of 10:1 defining the electrochemical cell, as displayed in Fig. S1.

2.2. Fabrication of organic electrochemical transistors

The fabrication process of OECTs was reported previously (Liang et al., 2018), including the metallization, passivation, and patterning of PEDOT:PSS forming the source-drain channel of the OECTs. The interdigitated OECTs (iOECTs) possessed a channel area of

95 μm × 30 μm. The PEDOT:PSS film had a thickness of 115 nm (Liang et al., 2019). 10% (v/v) DMSO and 1% (v/v) GOPS cross-linker were added into PEDOT:PSS to improve the polymer conductivity and enable a long-term operation of the device (Stavrinidou et al., 2013).

2.3. Electrode cleaning and preparation of aptamer-based sensors

The Au macroelectrode (ME) was firstly annealed with a hydrogen flame to remove the organic contaminations from the surface. Then, it was immersed into ethanol for 5 min and rinsed by MilliQ water. Oxidation and reduction scans were preformed over the potential −0.15 V–1.55 V (30 scans at a scan rate of 1 V/s and step width of 0.01 V) for final electrochemical cleaning. Prior to modifying the clean electrode with the thiolated Fc-tagged aptamer, the DNA oligomer stock solution was pretreated with 10 mM tris(2-carboxyethyl)phosphine hydrochloride (TCEP) for 1 h to cleave the disulfide bond of the ssDNA receptors. Afterwards, the solution was diluted to the desired aptamer concentration in 10 mM high salt concentration phosphate buffered saline (PBS, 1.5 M NaCl, 1 mM $MgCl_2$, pH = 7.4) and applied on the respective gold electrode for 16 h at room temperature to obtain the self-assemble monolayer via thiol-gold bonds. A final concentration of 0.5 μM aptamer was used for the incubation on the electrode. Physisorbed excess molecules were removed by rinsing the electrodes separately with 10 mM tris(hydroxymethyl)aminomethane (tris) buffer and consecutively with MilliQ for 3 times. Then, the electrode was incubated in 1 mM MCH/MilliQ solution for 1 h to completely block the electrode surface and avoid the formation of pinholes in the self-assembled monolayer (Boubour and Lennox, 2000). The excess MCH molecules were rinsed by MilliQ for three times followed by 10 mM tris buffer for another three times. For the regeneration measurement, the aptamer-modified electrode was immersed in hot tris buffer (~90 °C) for 10 min to unfold the aptamer sequence followed by rinsing with MilliQ water to wipe out the rudimental ATP. The electrodes were finally immersed in tris buffer for electrochemical measurements.

2.4. Electrochemical characterization

All electrochemical measurements with the above-mentioned electrodes were carried out in a conventional three-electrode setup using an Autolab potentiostat PGSTAT302 (Eco Chemie, Netherlands). A platinum wire with a size larger than the working electrode was employed as the counter electrode. A micro Ag/AgCl electrode with 3 M KCl (Micro DRIREF-450, World precision instruments, USA) was chosen as the reference electrode. The gold macroelectrode was used as working electrode. The surface area of the working electrode was determined by analyzing the area of the reduction peak from an oxidation/reduction cycle recorded by cyclic voltammetry (CV) in 50 mM H_2SO_4 electrolyte at a scan rate of 0.1 V/s (Schröper et al., 2008). The surface area of the electrode can be estimated according to $A = C/386\ (\mu C \cdot cm^{-2})$, where C is the area of gold oxide reduction peak.

The binding events of targets were analyzed by alternating current voltammetry (ACV) over the potential range of −0.2 V–0.8 V (vs. Ag/AgCl) at an AC frequency of 10 Hz and AC potential amplitude of 50 mV. The relationship between the surface coverage of the sensor electrode and the ACV peak current was previously established (D O'Connor et al., 1999) as:

$$I_{avg}(E_0) = \frac{2nf\,FN_{total}\sinh\left(\frac{nFE_{ac}}{RT}\right)}{\cosh\frac{nFE_{ac}}{RT} + 1} \quad (1)$$

where $I_{avg}(E_0)$ is the average ac peak current, n is the number of electrons transferred per redox event and equal to 1 for the Fc label, F is the Faraday constant, N_{total} is the number of redox species in the surface layer in mol, R is the universal gas constant, and T is the temperature. Different concentrations of ATP targets were obtained by dissolving the ATP powder in 10 mM tris buffer. The aptamer-modified electrodes were then incubated in the target electrolytes for 30 min. Prior to the measurements, the incubated electrodes were rinsed by tris buffer for 3 times. The detection of other ATP analogs, such as cytidine triphosphate (CTP), guanosine triphosphate (GTP), thymine triphosphate (TTP), and uridine triphosphate (UTP) followed similar procedures.

2.5. Electrical characterization of iOECTs

For the measurement of the output characteristic of iOECTs, the drain-source voltage (V_{ds}) was swept from −1 V to 0.2 V at a gate-source voltage (V_{gs}) varying from −0.5 V to 1.0 V with a step width of 0.1 V. An Ag/AgCl pellet (E−206, Sciency-products GmbH, Germany) was used as pseudo-reference electrode. The output and transfer characteristics of iOECTs with modified gate electrode was recorded by a Keithley 4200 semiconductor analyzer (Tektronix, SÜSS MicroTec, Germany) with four Source-Measure Units and a home-made amplifier system. The V_{ds} was set to −50 mV with sweeping V_{gs} from −0.5 V to 1.0 V to record the transfer characteristics. To detect the ATP by means of the OECT, the Au macroelectrode was employed as pseudo-reference electrode. All the measurements were performed by using 10 mM tris buffer in ultrapure water (MilliQ, Merck Millipore, Germany). The average and standard deviations were obtained from the measurements of three independently electrodes or iOECTs.

3. Results and discussion

3.1. Macroelectrode as aptasensor

The surface area of the macro-electrodes (ME) was determined by cyclic voltammetry in 50 mM H_2SO_4 electrolyte to be approximately 2.2 mm^2. The ATP aptamer was covalently attached on the gold electrode via a thiol-gold bond (Fig. S5 and Fig. S7) with a surface density of approximately 1.78×10^{13} molecules/cm^2 (Fig. S6). For the target detection, an ATP incubation time of 30 min was chosen, which was reported to provide stable, time-independent redox signals for ME (Feng et al., 2015b). In the absence of ATP target, the immobilized aptamer is randomly folded and the ferrocene (Fc) redox probe possesses a large averaged distance from the electrode surface (Fig. 1a). Consequently, the charge transfer distance for the oxidation/reduction of Fc group is very large and the corresponding cyclic voltammogram is dominated by capacitive charging currents, Fig. 2a. The addition of ATP targets (1 mM) induces a conformational change of the aptamer receptors due to target binding and the terminal Fc group comes closer to the electrode. This causes an enhancement of the electron transfer between redox probe and electrode surface which resulted in the presence of a redox peak (oxidation/reduction of the Fc group at ~0.3 V vs. Ag/AgCl). However, the peak is not very prominent in comparison to the charging current, which renders a quantitative analysis of the concentration dependence difficult. Alternatively, alternating current voltammetry (ACV) was employed to characterize the sensor performance of the macro electrode, Fig. 2b. This method can suppress the charging current and is, therefore, more sensitive to redox processes taking place at the electrode surface, even for samples with low receptor coverage (Feng et al., 2012). The ACV measurements exhibited a strong dependence of the peak current (approximately 0.25 V vs. Ag/AgCl) on the ATP concentration, which was varied from 0 M to 1 mM, Fig. 2c. A small but apparent peak was observed also in the absence of ATP, which can be explained by the structural flexibility of the aptamer strand (Xiao et al., 2005b; Zuo et al., 2007). To evaluate the response of the ME-aptasensor and exclude the influence of background signal (aptasensor without targets), the relative faraday current change was employed and presented as $(I_{target}\text{-}I_{apt\text{-}AuE})/I_{apt\text{-}AuE}$, where $I_{apt\text{-}AuE}$ is the redox current of the aptamer modified electrode before ATP binding. A steep and linear increase at the presence of low concentration of ATP targets between 100 nM and 1 μM (limit of linearity) is observed for the semi-logarithmic calibration curve (Fig. 2d). The signal of target at the

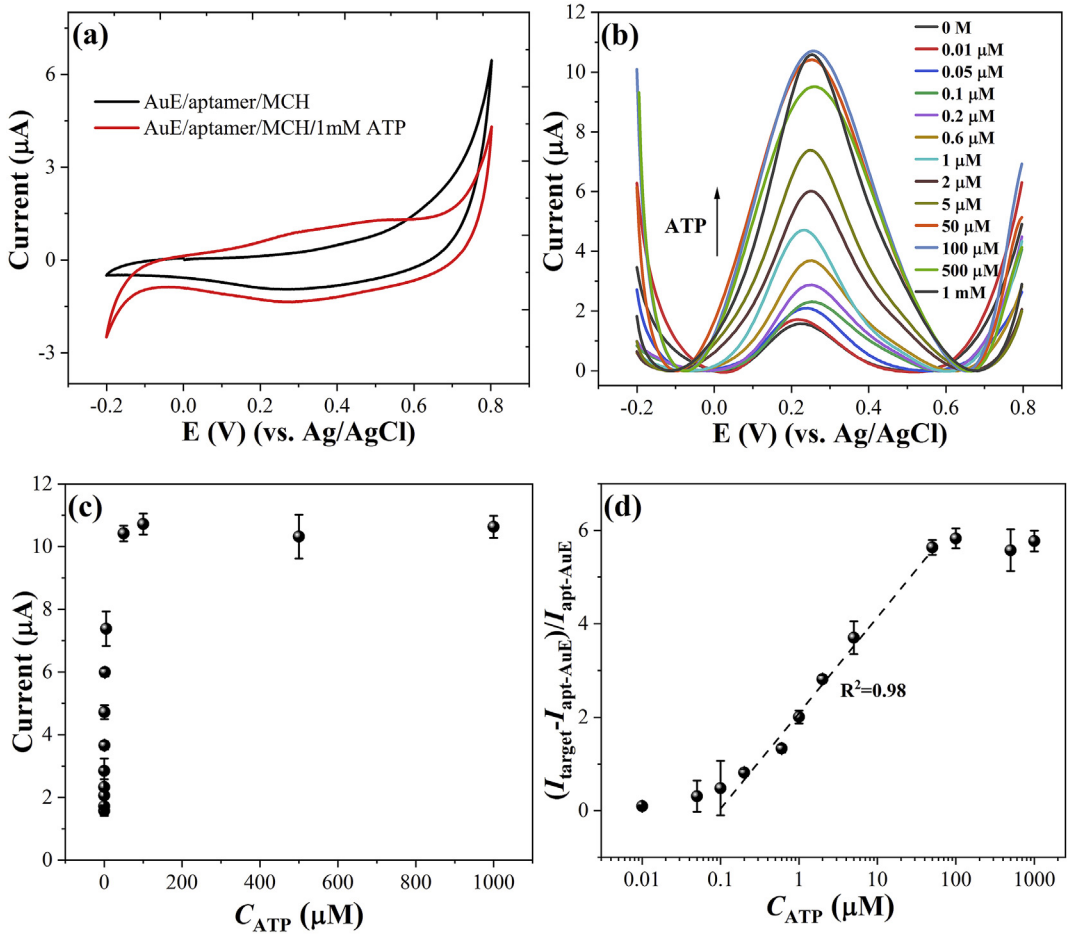

Fig. 2. (a) Cyclic voltammetry curves of an aptamer-modified macro electrode (black) and after incubation in 1 mM ATP solution (red). (b) ACV current responses of the aptamer-modified electrode with different ATP concentrations ranging from 0 μM (black curve) to 1 mM. Dependence of (c) the electrochemical current and (d) the relative current signal on ATP concentration.

limit of detection (S_{lod}) can be calculated according to the equation: $S_{lod} = S_{reag} + 3\sigma_{reag}$, where S_{reag} is the mean signal for reagent blank and σ_{reag} is the standard deviation for the signal of reagent blank. The resulting limit of detection (LOD) is 106 nM, which is comparable to previously reported aptamer-based ATP sensor (Feng et al., 2015b; Kashefi-Kheyrabadi and Mehrgardi, 2012, 2013; Lu et al., 2010). In addition, the dependence of electrochemical current on ATP concentration could also be fitted by a Langmuir-Freundlich equilibrium model allowing conclusions about the analyte coverage at a given concentration and the K_D of the receptor, Fig. S8.

3.2. Transfer characteristics of interdigitated organic electrochemical transistors

Organic electrochemical transistors (OECTs) have been well acknowledged as promising amplifying transducers for electrophysiology (Braendlein et al., 2017a). In the present work, interdigitated electrode arrays were utilized as source and drain electrodes and the conducting polymer poly(3,4-ethylenedioxythiophene) doped with poly(styrene sulphonate) (PEDOT:PSS) with a film thickness of 115 nm was chosen as active channel material to fabricate interdigitated OECTs (iOECT) for electrochemical sensing, Fig. 3a–b. The output characteristics of an iOECT with a drain-source bias (V_{ds}) in the range of −1.0 V–0.2 V and a gate-source bias (V_{gs}) varying from −0.5 V to 1.0 V was measured using a standard Ag/AgCl electrode as gate, Fig. 3c. The output drain-source current (I_{ds}) decreased with increasing V_{gs} especially when V_{gs} is above 0.1 V at constant V_{ds}. OECT are electrolyte-gated transistors and the active channel material can directly exchange charge carriers with the electrolyte (Bernards and Malliaras, 2007). Once a positive bias is applied at the gate electrode, cations from the electrolyte can penetrate into the PEDOT:PSS-based channel and compensates the pendant sulphonate anions on the PSS, which de-dopes the PEDOT, thus the doped PEDOT resulting in a decrease of the hole density in the conducting polymer channel, Fig. 3a (Khodagholy et al., 2013b). The capability of OECTs to convert the variation of gate potential into modulations of the output I_{ds} is given by the transconductance (g), defined as $g = \frac{\Delta I_{ds}}{\Delta V_{gs}}$ (Rivnay et al., 2013), a crucial transistor parameter governing the signal amplification (Khodagholy et al., 2013b). The transfer characteristics and the resultant transconductance at $V_{ds} = -0.5$ V were measured, as shown in Fig. 3d. Here, the iOECT were operated in a depletion mode with a drain-source current on-to-off ratio of 6.3×10^4, which is superior or comparable to other previously reported OECTs (Liang et al., 2018; Rivnay et al., 2013). The obtained maximum transconductance with respect to V_{ds} is close to 18 mS/V, outperforming other state-of-the-art transistors, such as graphene- (4.2 mS/V) (Ohno et al., 2009) and silicon nanowire transistors (167 μS) (Li et al., 2013a). However, it should be noted that the transconductance depends on many device specific parameters and a comparison can not take all aspects into account to make them fully comparable. Especially the channel thickness is very different for these three systems. A more detailed comparison can be found elsewhere (Khodagholy et al., 2013b). Also the OECT transconductance critically depends on the thickness of organic channel material and the width-to-length ratio of channel (Liang et al., 2019; Rivnay et al. 2013, 2015).

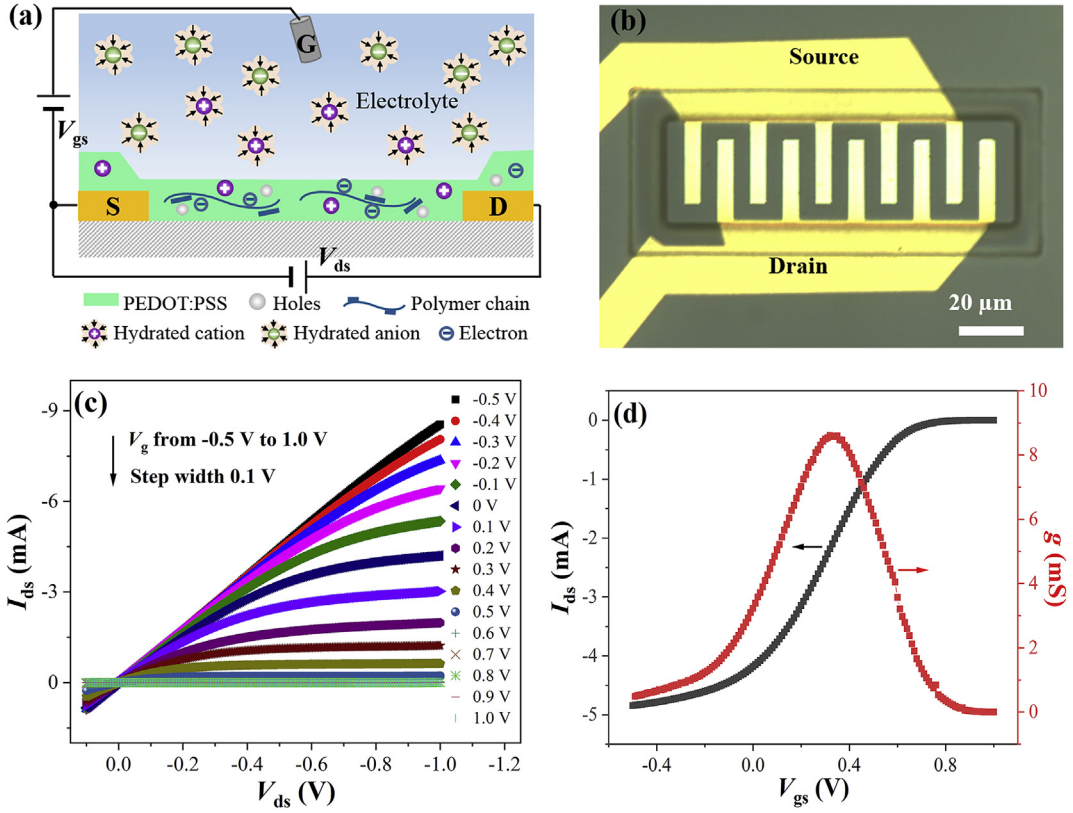

Fig. 3. (a) Schematic of the cross-section of an iOECT and its wiring diagram. An Ag/AgCl wire immersed into electrolyte is used as a gate electrode. (b) Optical micrograph of the source-drain channel of an iOECT. (c) The output characteristics of iOECTs for gate-source voltages (V_{gs}) varying from −0.5 V to 1.0 V with a step width of 0.1 V. (d) The transfer characteristics and the corresponding transconductance of iOECTs at a drain-source voltage (V_{ds}) = −0.5 V.

The interdigital architecture endows iOECTs (channel area: 95 μm × 30 μm) with high channel width-to-length ratio (W/L = 58) without sacrificing the transistor density on the device. As a result, the high transconductance renders possible the outstanding amplification capabilities of iOECT, a precondition for the following biosensor application. In addition, the output and transfer characteristics of iOECT with Au as gate electrode were recorded, which exhibited a similar response as that obtained by using typical Ag/AgCl electrode as gate, Fig. S3. The transconductance/V_{gs} curve for different electrolyte solutions also indicated that the buffer composition can influence the device performance, Fig. S4. Thus, the same buffer composition (10 mM tris buffer, pH = 7.4) was chosen as buffer solution for the following measurements.

3.3. OECTs as aptasensor

As mentioned previously, the low number of receptors in the self-assembled monolayer of the gold electrode correspondingly leads to small current signals for amperometric sensors. An alternative sensor concept links the aptamer receptors with organic electrochemical transistors, which facilitate intrinsic signal amplification due to their high transconductances. Previous work proposed that the surface potential, size (Cicoira et al., 2010), and material (capacitance) (Tarabella et al., 2010) of the gate electrode significantly affected the performance of OECTs. Therefore, the incubation of aptamer and the following specific binding with ATP on the gate electrode are assumed to affect the transfer characteristics of OECTs. To allow a direct comparison of the performance of amperometric and iOECT transducer, the same MEs as mentioned above were used as the gate electrode for the iOECTs. Also, the modification of the ME was done exactly the same as for the amperometric detection, section 3.1, and immersed together with the iOECT in the same analyte solution. The amperometric sensor used the redox peak current as a signal to determine the analyte concentration (Fig. 2), while the iOECT-based aptasensor measures the potential change of the gate electrode as a function of ATP concentration, Fig. 4. The transfer characteristics of iOECT with AuE/aptamer/MCH as gate electrode was recorded in tris buffer for different times. It was found that there is slight shift of gate voltage to lower potential after the immersion of iOECTs in electrolyte (Fig. S9 and Fig. S10). The transfer characteristics of the device before and after incubation with aptamer as well as after administration of different concentrations of ATP were recorded at a source drain bias of V_{ds} = −0.05 V. To determine the response of iOECTs to different concentrations of the targets, the ratio of the source-drain current before and after analyte administration $I_{ds}/I_{ds,on}$ is used (Fig. S10) due to the electrical instability of PEDOT:PSS film in electrolyte for long-term measurements (Fig. S9). The transfer curve significantly shifts horizontally towards higher gate voltages after the immobilization of aptamer on the bare gold electrode (Fig. 4a). Also, the addition of even 100 fM ATP to the electrode causes a shift of the transfer curve for approx. 5 mV to a higher gate voltage. A further increase of the ATP concentration to 2 pM results in an additional shift (~7 mV) of the gate voltage (Fig. 4a). The variation of the gate voltage is caused by even very small analyte concentrations, which indicate that few binding events can be monitored by the iOECT. The sensitive response originates from the high transconductance so that a minor change on the gate voltage leads to a pronounced alteration of channel current. These shifts of the gate voltage are reproducible but smaller than the detection limit since the relative changes eliminate the device variations (Table S1). Similarly, measurements with higher concentration of ATP were conducted by testing at least three samples for each condition (Fig. 4b and Table S1). The higher the concentration of the analyte, the bigger is the observed shift of gate/source biases. For example, the incubation in 1 nM ATP (far below the detection limit of the amperometric sensor) solution resulted in a change of the gate voltage,

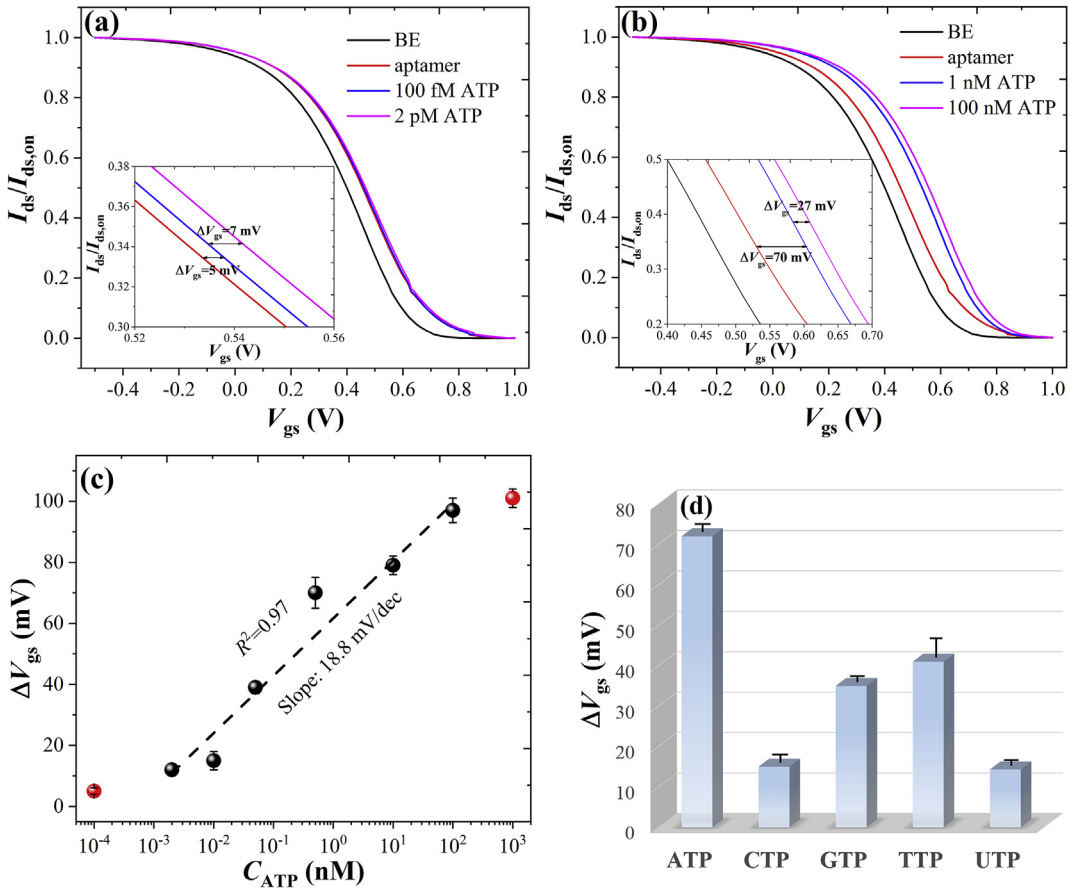

Fig. 4. Transfer characteristics of iOECTs versus gate voltage at $V_{ds} = -50$ mV, on bare gold electrode (BE), after incubation in aptamer solution and administration of the ATP target with different concentrations. (a) Concentration of ATP target in tris buffer was 100 fM and 2 pM. The target incubation time was 30 min. (b) Same conditions as a) but with ATP concentrations of 1 nM and 100 nM. The insets in (a) and (b) display the horizontal shift of transfer curves after incubation in aptamer solution and different concentration of ATP. (c) The gate potential shift of iOECTs after incubation for different concentrations of ATP. (d) Column comparison graph of the gate potential changes obtained for incubation of ATP (1 nM) and different analogs (1 μM) from the transfer characteristics of OECTs at $V_{ds} = -50$ mV indicated in Fig. S11.

approx. 70 mV.

From the shift of the gate voltage corresponding to different concentrations of ATP, a calibration curve was derived, Fig. 4c. The change of gate voltage (ΔV_{gs}) declines with the decrease in the concentration of ATP targets and an extremely low detection limit 100 fM is obtained with the minimum shift of gate voltage for 5 mV. A typical S-shaped curve is observed, which can be divided into three regimes. A sub-threshold regime for low ATP concentrations ($C_{ATP} \leq 100$ fM), where ΔV_{gs} was almost zero and independent of the measured concentration. In the second regime (2 pM $< C_{ATP} <$ 100 nM), ΔV_{gs} increased with the ATP concentration and the resulting sensitivity can be extracted from the slope of the fitting curve. This regime is followed by a third one for high analyte concentration where the corresponding ΔV_{gs} saturated. The logarithmic relationship between the change of gate voltage and the ATP concentration in the second regime showed a linear response ($R^2 = 0.97$) in a wide concentration range and a slope of 18.8 mV/decade, which represents the sensitivity of iOECTs for ATP sensing. The LOD for iOECT-based aptasensor is calculated using the same method as that for amperometric aptasensor. The resulting LOD is 10 pM. It is noteworthy that the LOD was determined based on absolute values of V_{gs} at $I_{ds}/I_{ds,on} = 0.5$, while the relative changes were used to extract the calibration curve, which are more reproducible since device related variations of the transfer characteristic are eliminated. The detection limits of several other previously reported aptamer-based ATP sensors are summarized and compared to the iOECT sensor in Table 1. The detection limit to ATP in ACV measurement of the ME-aptasensor is only about 106 nM ± 13.7 nM, which is nearly 4 orders of magnitude higher than that of the iOECT-based aptasensor (10 pM). The latter is more sensitive than most of other reported electrochemical ATP aptasensors, which exhibited detection limits not smaller than 20 pM. The ultralow detection limit of iOECTs in ATP sensing could be attributed to the inherent amplification effect of transistors (Fu et al., 2017). Apart from the sensitivity, the other crucial parameter to evaluate the performance of aptasensor is the selectivity. Due to the specific binding properties of aptamers, the selective response to ATP over other organic triphosphate analogs, such as cytidine triphosphate (CTP), guanosine triphosphate (GTP), thymine triphosphate (TTP), and uridine triphosphate (UTP), was characterized (Fig. S11 and Fig. 4d). The variations of gate potentials caused by the unspecific binding of ATP analogs is smaller (less than 40 mV) than the specific signal (approx. 70 mV) although the concentration of the former (1 μM) was 1000 times higher than that of ATP (1 nM), confirming the high selectivity of the aptasensor reported before (Feng et al., 2015b).

To characterize the thermo-stability and reusability of the aptasensor, regeneration tests were performed for both amperometric (Fig. 5a and Fig. S12) and iOECT-based aptasensor (Fig. 5b). Therefore, a consecutive detection of 100 μM ATP was done after soaking the sensor in hot tris buffer (approx. 90 °C). The temperature treatment unfolded the ssDNA aptamer molecules and released the ATP ligand(Xia et al., 2013). After this regeneration treatment, the ACV current drops to 3.2 μA, close to the background signal (2.8 μA), Fig. 5a. Subsequent detection tests for 100 μM ATP showed similar responses as the freshly

Table 1
Comparison of sensor performance of iOECTs with other reported sensors for ATP detection.

	Transducer	Detection limits	Detection solution	Detection range/ decades	References
Electroche-mical aptasensor	Silver nanoparticles	1 μM	10 mM PBS (pH = 7.4) containing 5.0 mM $[Fe(CN)_6]^{3-/4-}$ and 0.1 M KCl.	3	Kashefi-Kheyrabadi and Mehrgardi (2012)
	Graphene-modified electrodes	20 pM	100 mM citrate–phosphate buffer (pH 7.0)	5	Sanghavi et al. (2013)
	Electrochemical current rectification	114 nM	10 mM PBS (pH = 7.4)	3	Feng et al. (2015b)
	Nanoporous gold	100 nM	10 mM PBS (pH = 7.0)	4	Kashefi-Kheyrabadi and Mehrgardi (2013)
	polydopamine-silver nanoclusters nanoplatform	0.01 pM	10 mM PH = 7.0 PBS	5	Zhang et al. (2019)
Other methods	Catalytic recycling	50 nM	20 mM tris-HCl buffer (pH = 7.4)	3	Lu et al. (2010)
	Surface plasmon resonance	10 nM	10 mM PBS (pH = 7.4)	3	Xie et al. (2014)
	Electrochemiluminescence sensor	1.5 nM	10 mM PBS (pH = 7.4)	3	Lu et al. (2013)
		8 nM	100 mM PBS (pH = 9.0)	3	Liu et al. (2014)
Present work	ME	106 nM	10 mM tris buffer, (pH = 7.4)	3	
	iOECTs	10 pM		5	

prepared sensor, indicating that the aptamer receptor itself as well its surface tether remained mainly unaffected by this hot buffer treatment. After three detection cycles, the sensor response exhibited ~90% of the initial value. However, V_{gs} at $I_{ds}/I_{ds,on} = 0.5$ fluctuates to a certain extent for both regeneration and target-binding, Fig. 5b. Nevertheless, this is the first report about the regeneration of an OECT sensor to the best of our knowledge. Most previous work on OECT biosensors reported on single use only since they used antibody or enzymatic receptors (Fu et al., 2017; Liao et al., 2015), which easily denature during harsh regeneration treatments.

Previous work proposed that the channel current response of OECTs to analyte species can be attributed to changes of the effective gate voltage. Different from the detection of glucose (Bernards et al., 2008; Tang et al., 2011b), dopamine (Liao et al., 2014; Tang et al., 2011a), and uric acid (Liao et al., 2015) where electrochemical reactions occur at the interfaces of gate electrode and PEDOT:PSS channel, the working mechanism for ATP sensing investigated here is based on the modulation of the gate electrode surface potential due to target binding (Fig. 5c). Considering the characteristics of OECTs (Bernards et al., 2008; Bernards and Malliaras, 2007), no charge transfer occurs at the electrodes for gate voltages lower than 1.25 V and the double layer between Au electrode and electrolyte can be regarded as a capacitor. Consequently, the channel current of OECTs can be described as:

$$I_{ds} = G\cdot\left[1 - \frac{V_g^{eff} - 0.5V_{ds}}{V_p}\right]\cdot V_{ds} \tag{2}$$

$$V_p = qp_0 d\cdot\frac{(C_{GE} + C_{EC})WL}{C_{GE}C_{EC}} \tag{3}$$

where $G = q\mu p_0 Wd/L$, is the conductance of the polymer channel, V_p is the pinch-off voltage, C_{GE} is the capacitance of the interface between gate electrode and electrolyte, C_{EC} is the capacitance of the interface between channel and electrolyte, W and L are the width and length of the semiconducting polymer channel, respectively, d is the thickness of the active layer, q is the elementary charge, p_0 is the initial hole density in the active layer before the application of gate voltage, and μ is the hole mobility (Bernards et al., 2008; Bernards and Malliaras, 2007). V_g^{eff} is the effective gate voltage, which is given by: $V_g^{eff} = V_g + V_{offset}$. The V_{offset} is the offset voltage of OECTs, which is related to the potential drop at the two electrochemical double layers: gate/electrolyte and electrolyte/drain-source channel.

The modulation of the channel current caused by the binding events can be ascribed to the change of the offset voltage by $\Delta\psi$ at the gate electrode. At neutral pH, the ssDNA aptamers and ATP are negatively charged. Consequently, both aptamer immobilization and subsequent ATP binding reduce the surface potential of the Au electrode. The change of potential can be estimated by (Thompson et al., 2005):

$$\Delta\psi = \frac{nQ_{apt}}{\varepsilon_r\varepsilon_0}\cdot d_{apt} \tag{4}$$

where n is the density of aptamer molecules on the surface of the gate electrode, Q_{apt} is the charge of a single aptamer molecule, ε_r is the relative permittivity of aptamers, ε_0 is the dielectric permittivity of the free space, and d_{apt} is the thickness of aptamer layer. Therefore, to maintain the same V_g^{eff}, a higher gate voltage needs to be applied to compensate the potential shift induced by the binding event. With the increase in ATP concentration, rising gate potentials are needed, which shifts the gate voltage until it reaches the saturation regime of the OECT (Rivnay et al., 2015). Since the applied effective gate voltage on the organic channel material is same, the resultant I_{ds} is unchanged but the corresponding V_g shifts to higher potential compared to the case before the binding events. As a result, the capability to convert the modulation of gate voltage into rising channel current declines. According to the above-mentioned working mechanism of iOECTs for ATP detection, it can be concluded that the modification of aptamer by expensive redox

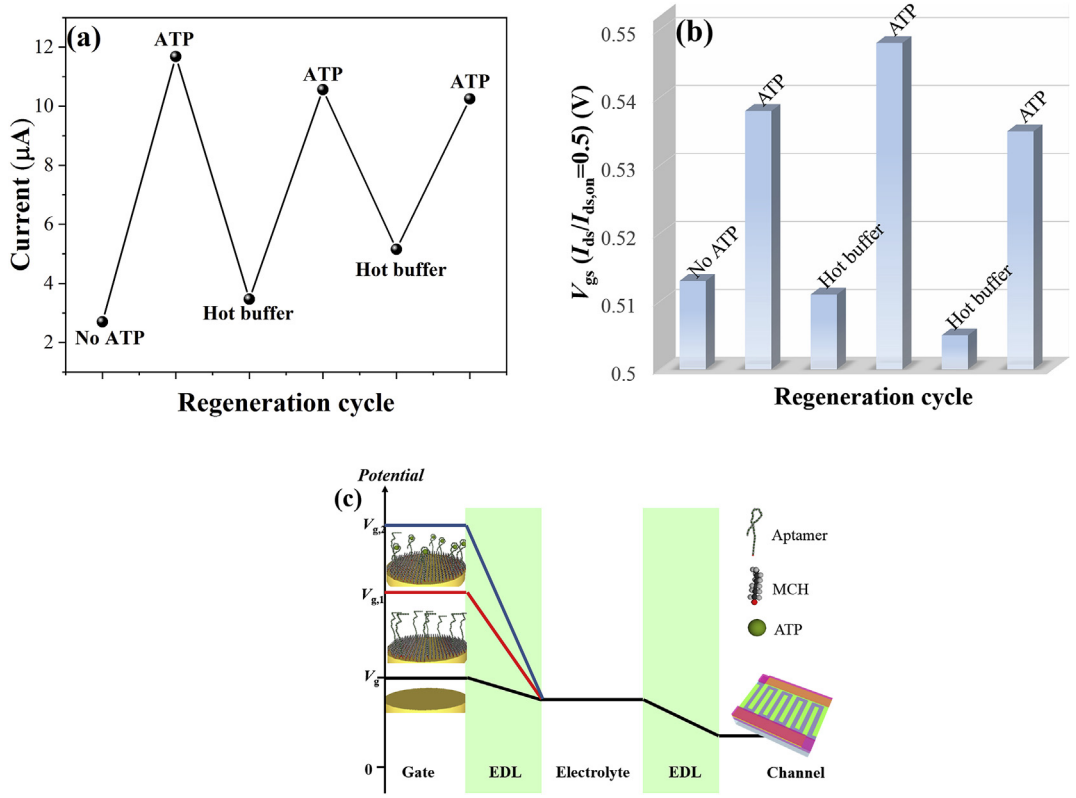

Fig. 5. (a) ACV current responses (symbols) and (b) the corresponding values of V_{gs} at $I_{ds}/I_{ds,on}$ = 0.5 extracted from the transfer characteristics of iOECTs showing the regeneration of aptasensors after repeated washing the amperometric aptasensor with hot tris buffer. (c) Schematic diagram of potential drops of iOECTs for bare gold electrode (V_g), after incubation in aptamer solution and 1 mM MCH solution ($V_{g,1}$), and after administration of ATP ($V_{g,2}$).

probe is not needed for OECT-based aptasensors to obtain changes of gate potential by analyte binding events.

The influence of the change of the electrolyte composition on the electrolyte resistance and the electrolyte PEDOT/PSS channel interface is negligible in comparison to the gate potential shift in our case because of the following reasons. Firstly, the gate-source leakage current is in the range of several nA (Fig. S14) while the source-drain current has mA. Consequently, variations of the electrolyte resistance due to changes of the sample composition can be neglected. Secondly, our iOECTs exhibited a significantly different sensitivity for variations of the cation concentration than the ATP concentration, Fig. S13. A logarithmic dependence between the changes of gate potential (Fig. S13b) and ion concentration is obtained, with the slope of 71.7 mV/decade for K^+ and 60.4 mV/decade for bivalent magnesium Mg^{2+} (Lin et al., 2010a). Compared to the shallow slop (18.8 mV/decade) for ATP detection, it can be assumed that the high ions-sensitivity of OECTs (71.7 mV/decade for K^+) is based on a channel dependent mechanism involving doping/dedoping processes. Thus, the change in effective gate voltage in the latter is mainly attributed to a potential change occurring at the interface of electrolyte and PEDOT:PSS channel. The offset voltage for the device at different concentration of ions in the electrolyte is given by equation (5) according to Bernard et al. (Bernards et al., 2008):

$$V_{\text{offset}} = \text{A} + \left(1 + \frac{C_{\text{EC}}}{C_{\text{GE}}}\right)\frac{\text{k}T}{ne}\ln[\text{M}^{n+}] \quad (5)$$

where $[M^{n+}]$ is the cation concentration in the electrolyte, A is a constant, k is Boltzmann's constant, T is the temperature, n is the number of electrons transferred to neutralize $PEDOT^+$, and e is the electron charge. Consequently, it can be assumed that V_{offset} is caused rather by $\Delta\psi$ associated to binding events happening at the gate electrode than OECT channel related processes.

4. Conclusions

In this work, a novel strategy to detect a very light molecule (ATP) without involving any kind of catalytical amplification is proposed. The signal of a conventional amperometric aptamer sensor is converted and compared to responses of a potentiometric iOECT transducer. Therefore, amperometric biosensor, composed of an aptamer-modified electrode is linked as gate to an interdigitated OECT circuit. The actual binding process of ATP to the aptamer receptors is practically the same for both transducer systems. Nevertheless, the iOECT transducer possessed an ultralow detection limit of 10 pM, which is four orders of magnitude lower than that of the amperometric system and even superior to most of previously reported electrochemical detection approaches. The potentiometric transducer successfully converted variations of gate potential caused by the binding event between analyte and receptor into an alteration of PEDOT:PSS channel current benefiting from the high transconductance and the corresponding amplification properties of iOECTs. The iOECT-based aptasensors were sensitive enough to differentiate ATP from other organic triphosphate analogs and can be easily regenerated by unfolding the aptamer sequence in hot buffer solution, demonstrating the versatility of OECTs for aptasensor usage. The simple assembly and operation of the integrated iOECTs as aptasensors facilitates the transfer of this concept to many previously reported electrochemical aptamer-based sensors, which usually do not possess any signal amplification and are therefore restricted regarding detection limit and detection range. This is the case in particular for the detection of light molecules, like Aβ oligomers, where ultralow detection limits are required.

CRediT authorship contribution statement

Yuanying Liang: Investigation, Formal analysis, Writing - original

draft. **Changtong Wu:** Investigation. **Gabriela Figueroa-Miranda:** Investigation. **Andreas Offenhäusser:** Conceptualization, Funding acquisition, Project administration. **Dirk Mayer:** Conceptualization, Data curation, Formal analysis, Validation, Supervision, Writing - review & editing.

Declaration of competing interest

The authors declare that they have no known competing financial interests or personal relationships that could have appeared to influence the work reported in this paper.

Acknowledgements

The devices were fabricated in the Helmholtz Nano Facility of Forschungszentrum Jülich. We thank the Federal Ministry of Education and Research (Germany), funding code 031A095B and Yuanying Liang is grateful for the financial support from the China Scholarship Council (201506240059). Gabriela Figueroa-Miranda is grateful for the scholarship of the Mexican National Council for Science and Technology (CONACyT) and the German Academic Exchange Service (DAAD, grant number: 448904).

Appendix A. Supplementary data

Supplementary data to this article can be found online at https://doi.org/10.1016/j.bios.2019.111668.

References

Bernards, D.A., Macaya, D.J., Nikolou, M., DeFranco, J.A., Takamatsu, S., Malliaras, G.G., 2008. J. Mater. Chem. 18, 116–120.
Bernards, D.A., Malliaras, G.G., 2007. Adv. Funct. Mater. 17, 3538–3544.
Boubour, E., Lennox, R.B., 2000. Langmuir 16, 4222–4228.
Braendlein, M., Lonjaret, T., Leleux, P., Badier, J.M., Malliaras, G.G., 2017a. Adv. Sci. 4, 1600247.
Braendlein, M., Pappa, A.-M., Ferro, M., Lopresti, A., Acquaviva, C., Mamessier, E., Malliaras, G.G., Owens, R.M., 2017b. Adv. Mater. 29, 1605744.
Chen, L., Fu, Y., Wang, N., Yang, A., Li, Y., Wu, J., Ju, H., Yan, F., 2018. ACS Appl. Mater. Interfaces 10, 18470–18477.
Cicoira, F., Sessolo, M., Yaghmazadeh, O., DeFranco, J.A., Yang, S.Y., Malliaras, G.G., 2010. Adv. Mater. 22, 1012–1016.
D O'Connor, S., Olsen, G.T., Creager, S.E., 1999. J. Electroanal. Chem. 466, 197–202.
E Wang, R., Zhang, Y., Cai, J., Cai, W., Gao, T., 2011. Curr. Med. Chem. 18, 4175–4184.
Feng, J., Sun, X., Wu, C., Peng, L., Lin, C., Hu, S., Yang, J., Xie, Y., 2011. J. Am. Chem. Soc. 133, 17832–17838.
Feng, L., Lyu, Z., Offenhäusser, A., Mayer, D., 2015a. Angew. Chem. Int. Ed. 54, 7693–7697.
Feng, L., Lyu, Z., Offenhäusser, A., Mayer, D., 2016. Eng. Life Sci. 16, 550–559.
Feng, L., Sivanesan, A., Lyu, Z., Offenhäusser, A., Mayer, D., 2015b. Biosens. Bioelectron. 66, 62–68.
Feng, L., Zhao, C., Xiao, Y., Wu, L., Ren, J., Qu, X., 2012. Chem. Commun. 48, 6900–6902.
Fu, Y., Wang, N., Yang, A., Law, H.K.w., Li, L., Yan, F., 2017. Adv. Mater. 29, 1703787.
Gründler, P., 2007. Chemical Sensors: an Introduction for Scientists and Engineers. Springer Science & Business Media.
Kashefi-Kheyrabadi, L., Mehrgardi, M.A., 2012. Biosens. Bioelectron. 37, 94–98.
Kashefi-Kheyrabadi, L., Mehrgardi, M.A., 2013. Bioelectrochemistry 94, 47–52.
Khodagholy, D., Doublet, T., Quilichini, P., Gurfinkel, M., Leleux, P., Ghestem, A., Ismailova, E., Hervé, T., Sanaur, S.b., Bernard, C., 2013a. Nat. Commun. 4, 1575.
Khodagholy, D., Rivnay, J., Sessolo, M., Gurfinkel, M., Leleux, P., Jimison, L.H., Stavrinidou, E., Herve, T., Sanaur, S.b., Owens, R.M., 2013b. Nat. Commun. 4, 2133.
Kim, D.-J., Lee, N.-E., Park, J.-S., Park, I.-J., Kim, J.-G., Cho, H.J., 2010. Biosens. Bioelectron. 25, 2477–2482.
Lai, R.Y., Plaxco, K.W., Heeger, A.J., 2007. Anal. Chem. 79, 229–233.
Li, B.R., Chen, C.W., Yang, W.L., Lin, T.Y., Pan, C.Y., Chen, Y.T., 2013a. Biosens. Bioelectron. 45, 252–259.
Li, J., Yang, Z., Tang, Y., Zhang, Y., Hu, X., 2013b. Biosens. Bioelectron. 41, 698–703.
Liang, Y., Brings, F., Maybeck, V., Ingebrandt, S., Wolfrum, B., Pich, A., Offenhäusser, A., Mayer, D., 2019. Adv. Funct. Mater. https://doi.org/10.1002/adfm.201902085.
Liang, Y., Ernst, M., Brings, F., Kireev, D., Maybeck, V., Offenhäusser, A., Mayer, D., 2018. Adv. Healthc. Mater. 7, 1800304.
Liao, C., Mak, C., Zhang, M., Chan, H.L., Yan, F., 2015. Adv. Mater. 27, 676–681.
Liao, C., Zhang, M., Niu, L., Zheng, Z., Yan, F., 2014. J. Mater. Chem. B 2, 191–200.
Lin, P., Luo, X., Hsing, I., Yan, F., 2011. Adv. Mater. 23, 4035–4040.
Lin, P., Yan, F., Chan, H.L., 2010a. ACS Appl. Mater. Interfaces 2, 1637–1641.
Lin, P., Yan, F., Yu, J., Chan, H.L., Yang, M., 2010b. Adv. Mater. 22, 3655–3660.
Liu, Y., Lei, J., Huang, Y., Ju, H., 2014. Anal. Chem. 86, 8735–8741.
Lu, C.H., Li, J., Lin, M.H., Wang, Y.W., Yang, H.H., Chen, X., Chen, G.N., 2010. Angew. Chem. Int. Ed. 49, 8454–8457.
Lu, J., Yan, M., Ge, L., Ge, S., Wang, S., Yan, J., Yu, J., 2013. Biosens. Bioelectron. 47, 271–277.
Lubin, A.A., Plaxco, K.W., 2010. Acc. Chem. Res. 43, 496–505.
Ohno, Y., Maehashi, K., Yamashiro, Y., Matsumoto, K., 2009. Nano Lett. 9, 3318–3322.
Palchetti, I., Mascini, M., 2012. Anal. Bioanal. Chem. 402, 3103–3114.
Privett, B.J., Shin, J.H., Schoenfisch, M.H., 2010. Anal. Chem. 82, 4723–4741.
Rivnay, J., Leleux, P., Ferro, M., Sessolo, M., Williamson, A., Koutsouras, D.A., Khodagholy, D., Ramuz, M., Strakosas, X., Owens, R.M., 2015. Sci. Adv. 1, e1400251.
Rivnay, J., Leleux, P., Sessolo, M., Khodagholy, D., Hervé, T., Fiocchi, M., Malliaras, G.G., 2013. Adv. Mater. 25, 7010–7014.
Sanghavi, B.J., Sitaula, S., Griep, M.H., Karna, S.P., Ali, M.F., Swami, N.S., 2013. Anal. Chem. 85, 8158–8165.
Saraf, N., Woods, E.R., Peppler, M., Seal, S., 2018. Biosens. Bioelectron. 117, 40–46.
Schröper, F., Brüggemann, D., Mourzina, Y., Wolfrum, B., Offenhäusser, A., Mayer, D., 2008. Electrochim. Acta 53, 6265–6272.
Stavrinidou, E., Leleux, P., Rajaona, H., Khodagholy, D., Rivnay, J., Lindau, M., Sanaur, S.b., Malliaras, G.G., 2013. Adv. Mater. 25, 4488–4493.
Tan, W., Donovan, M.J., Jiang, J., 2013. Chem. Rev. 113, 2842–2862.
Tang, H., Lin, P., Chan, H.L., Yan, F., 2011a. Biosens. Bioelectron. 26, 4559–4563.
Tang, H., Yan, F., Lin, P., Xu, J., Chan, H.L., 2011b. Adv. Funct. Mater. 21, 2264–2272.
Tarabella, G., Santato, C., Yang, S.Y., Iannotta, S., Malliaras, G.G., Cicoira, F., 2010. Appl. Phys. Lett. 97, 205.
Thompson, M., Cheran, L.-E., Zhang, M., Chacko, M., Huo, H., Sadeghi, S., 2005. Biosens. Bioelectron. 20, 1471–1481.
White, R.J., Phares, N., Lubin, A.A., Xiao, Y., Plaxco, K.W., 2008. Langmuir 24, 10513–10518.
Xia, T., Yuan, J., Fang, X., 2013. J. Phys. Chem. B 117, 14994–15003.
Xiao, Y., Lai, R.Y., Plaxco, K.W., 2007. Nat. Protoc. 2, 2875.
Xiao, Y., Lubin, A.A., Heeger, A.J., Plaxco, K.W., 2005a. Angew. Chem. Int. Ed. 44, 5456–5459.
Xiao, Y., Piorek, B.D., Plaxco, K.W., Heeger, A.J., 2005b. J. Am. Chem. Soc. 127, 17990–17991.
Xie, L., Yan, X., Du, Y., 2014. Biosens. Bioelectron. 53, 58–64.
Zeglio, E., Inganäs, O., 2018. Adv. Mater. 30, 1800941.
Zhang, T., Xu, Z., Xu, H., Gu, Y., Xing, Y., Yan, X., Liu, H., Lu, N., Song, Y., Zhang, S., 2019. Sens. Actuators, B 288, 469–475.
Zuo, X., Song, S., Zhang, J., Pan, D., Wang, L., Fan, C., 2007. J. Am. Chem. Soc. 129, 1042–1043.